

Ba_{0.97}La_{0.02}Ti_{1-x}Nb_{4x/5}O₃ for $x = 0.07$ and 0.10 perovskite ceramics: effect of doping on electrical, dielectrical responses and conductivity mechanisms

M Jebli^{1*} , J Dhahri¹, N Hamdaoui², M A Albedah³, H Belmabrouk³ and M H Dhaou⁴

¹Laboratoire de la Matière Condensée et des Nanosciences, Département de Physique, Faculté des Sciences, Université de Monastir, 5019 Monastir, Tunisia

²ISITCom, University of Sousse, Gp1, 4011 Hammam Sousse, Tunisia

³Department of Physics, College of Science, Majmaah University, 11952 Al-Majmaah, Saudi Arabia

⁴Department of Physics, College of Science, Qassim University, Buraydah Almolaydah, Buraydah, Saudi Arabia

Received: 18 April 2023 / Accepted: 09 October 2023 / Published online: 14 November 2023

Abstract: The effect of Nb for Ti substitution on the electrical, modulus, dielectric and conductivity behaviors of a ceramic perovskite, barium lanthanum titanate (BLTi_{1-x}Nb_{4x/5}), Ba_{0.97}La_{0.02}Ti_{1-x}Nb_{4x/5}O₃, for $x = 0.07$ and 0.10 , was investigated at a 0 V d.c. bias potential. The flux reaction method was used to create our solid solutions. With a rising niobium amount, electrical conductivity rose. Jonscher's universal power law was used to fit the experimental results. The fact that the exponent n is marginally greater than 1 suggests that the hopping takes place between neighboring sites. As frequency rose, the dielectric constant dropped. Maxwell–Wagner (M-W) interface polarization is responsible for this behavior. Complex impedance spectroscopy was used to inspect the electrical characteristics in the frequency band (100–10⁶ Hz), at a 0 V d.c. bias potential. With increasing Nb concentration, the real and imaginary components of impedance rose. Each sample was represented by a single impedance semicircle on the complex impedance plot that was visible over both high and low frequencies. The measurement of the complex electrical modulus spectrum revealed the impact of grain boundaries and grains on electrical properties. A mismatch between the two maxima of the impedance and electrical modulus normalization curves was observed, which points to the possibility of short-range motion of charge carriers.

Keywords: Flux reaction; Electrical properties; Equivalent circuit analysis; Electric modulus spectroscopy; Electrode effects

1. Introduction

At room temperature, tetragonal BaTiO₃ is a ferroelectric perovskite (ABO₃) that is used as an overload protection mechanism in electrical products as well as a dielectric material in multilayer capacitors (MLCs). Dielectric materials must be electrically isolating ($> 10^{10} \Omega$) and have elevated permittivity values (> 1000) at room temperature in order to be used in MLC applications [1, 2]. They must experience a sharp increase in resistivity (~ 4 – 6 orders of magnitude) when heated above the ferro-

to-para-electric (tetragonal to cubic) phase transition temperature, T_c , in order to function as overload protection devices. At room temperature, they must be semiconducting ($> 100 \Omega$) [3].

These temperature-controlling mechanisms are referred to as positive temperature coefficient of resistance (PTCR) devices. At room temperature, this system is extremely resistive when pure, but some dopants, such as rare earth elements, can significantly reduce its electrical resistivity. Polycrystalline BaTiO₃ that has received donor doping can display PTC properties.

A- and B-site dopants have been used for many years to alter the electrical properties of BaTiO₃, but in many occasions, the doping mechanism(s) and defect chemistry

*Corresponding author, E-mail: marwaa.jebli12@gmail.com

are still unclear and/or debatable. Specifically, there has been much discussion about the doping process of La in BaTiO₃ [4, 5]. Since (> 0.5 atom%) (LaBa)TiO₃ ceramics made in air and quenched from 1350 °C exhibit semiconductivity, it is thought that La can function as a “donor” dopant under suitable circumstances.

In a limited composition range, from 0.2 to 0.4 mol% La, lanthanum can be added to BaTiO₃ to transform the material into a semiconductor [6]. In this study, the precursor powders for the synthesis of La doped-BaTiO₃, with 0.3 mol% La, were created using an oxalate-based coprecipitation method. This is a straightforward chemical precipitation method to produce fine particles with favorable physical properties for a quick sintering process. The A sites of the perovskite structure are occupied by lanthanum thanks to the use of a Ti excess. To investigate the preparation-affected PTC behavior, electrical measurements were made in the sintered samples.

The morphology and dielectric characteristics of BTNb ceramics were compared. BTNb’s crystal structure displayed less tetragonality. At room temperature, the analytical findings demonstrated that raising the Nb⁵⁺ concentration prevented abnormal grain development which determined a dielectric constant as 5200 [7].

For these technological uses, a controlled preparation of the compounds is necessary to optimize material performance. The flux method or molten salt method is one of the possible preparation methods, and it has the benefit of guaranteeing the chemical purity of the finished product—a crucial aspect that must be taken into account for electrical characteristics purposes.

Any ceramic system’s microstructure can be distinguished using the complex impedance spectroscopy (CIS) analysis [8]. Through this examination, it is possible to ascertain the contributions of different processes, including electrode interface, grain boundary and volume effects in the frequency domain [9]. An extensive range of temperatures and frequencies can be covered by this study.

Typically, complex impedance Z^* , complex admittance Y^* , complex modulus M^* and complex permittivity ε^* can be used to describe the data in the complex representation [10].

Based on previously published research results [10, 11], the goal of this paper is to examine the impact of the 5-valent (Nb⁵⁺) donor dopant on the conductivity mechanisms, dielectric and electrical responses as well as modulus study of Ba_{0.97}La_{0.02}Ti_{1-x}Nb_{4x/5}O₃ ceramics with $x = 0.07$ and 0.10 (noted BLTi_{0.93}Nb_{0.056} and BLTi_{0.90}Nb_{0.08}). Thus, there is a strong need for focus in this direction. As a result, we provide here a thorough analysis of the structural, conductivity, impedance, dielectric and modulus behavior of the solid solution of Nb-doped BLT against frequency (f), at nil d.c. bias

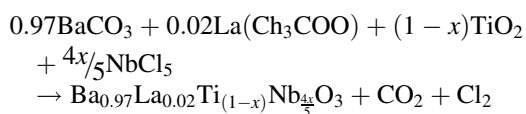
potential. Significant accomplishments include, interrelated to:

- XRD investigation reveals that our synthesized perovskite samples have a pure-tetragonal structure with the space-group P4/mmm.
- The electrical conductivity was studied, and exploratory data were fitted using the Jonscher’s universal power law.
- Depending on the frequency, the variation of ε' can be explained in terms of the attitude of interfacial polarization of the MW type, with nil d.c.-bias potential.
- The electrical characteristics of the prepared samples were examined using complex impedance spectroscopy.
- The Nyquist plot shows that both the grain and the grain border contribute to relaxation, with the grain boundaries being more resistive and capacitive than the grains.
- Modulus analysis demonstrates that relaxation in our samples is non-Debye, with nil d.c.-bias potential.

Additionally, the aim of this research is to create a ceramic composition that is lead-free, environmentally sustainable and essential for the production of electronic materials.

2. Sample preparation and experimental details

The flux reaction technique was used to create Ba_{0.97}La_{0.02}Ti_{1-x}Nb_{4x/5}O₃ ceramics with $x = 0.07$ and 0.10 (noted BLTi_{0.93}Nb_{0.056} and BLTi_{0.90}Nb_{0.08}). BaCO₃, TiO₂, NbCl₅ and LaCH₃CO₂ powders were combined in stoichiometric quantities and are all extremely pure (99.9%). The various precursor powders are thought to use an exactitude balancing under the stoichiometric requirements specified in the preceding synthesis condition:



After that, the combination of salt and precursor was put in an alumina crucible and heated for 24 h at 800 °C before being cooled to room temperature.

The mixture was washed with distilled water, filtered to eliminate the salts and then dried at 100 °C in the air following post-calcinations milling and extraction. In order to produce homogeneous and nano-polycrystalline powders, this procedure was repeated three times.

The powders were completely ground before being pressed into circular pellets with an 8 mm diameter and a few millimeters of thickness (~ 2 mm). The obtained

pellets were put into an alumina crucible and sintered for 24 h at 800 °C in the air. Figure 1 depicts the BLTi_{0.93}Nb_{0.056} and BLTi_{0.90}Nb_{0.08} synthesis flowchart that was used in this work.

A PANalytical X'Pert Pro diffractometer with Cu-Kα radiation ($\lambda = 1.54060 \text{ \AA}$) was used to record the X-ray diffraction patterns (XRD) and identify the phase purity, structure, space groups and lattice parameters of all prepared ceramics, at room temperature.

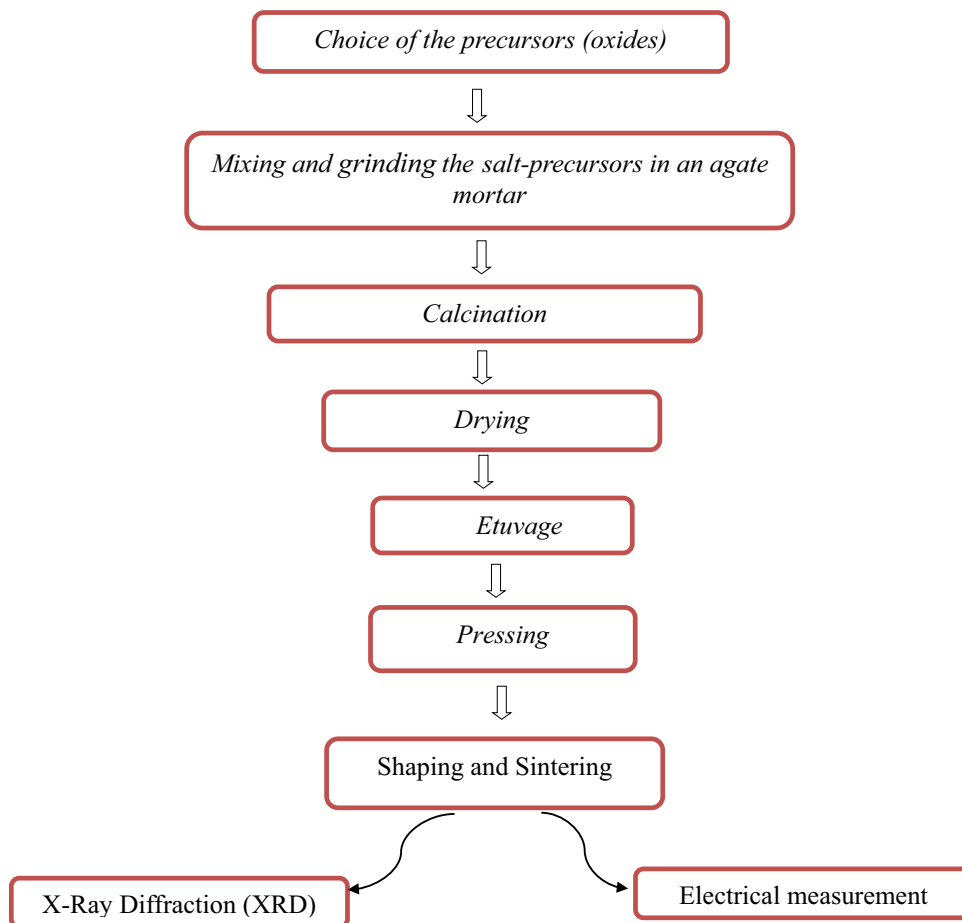
Using an Agilent 4294A at frequencies between 100 Hz and 5 MHz, the impedance and transport characteristics of the polycrystalline material were investigated.

3. Results and discussion

3.1. Structural investigation

From powder XRD studies, the structural characterization has been completed. BLTi_{1-x}Nb_{4x/5} (for x = 0.07 and 0.10) XRD patterns obtained at room temperature are indicative of a tetragonal structure with a P4/mmm space group [12]. The X-ray diffraction pattern for both ceramic materials is

Fig. 1 Flowchart illustrating the procedure for the preparation of BLTi_{0.93}Nb_{0.056} and BLTi_{0.90}Nb_{0.08} solid solutions



displayed in Fig. 2. In the earlier work [13], the structural characterization is described in more profundity.

The compositions have a single-pure-phase structure, which means that no secondary phase or impurity was detected in any of the polycrystalline samples. The intense and fine peaks in our samples indicate excellent crystallinity.

3.2. Electrical conductivity

Figure 3a displays the conductivity variance for x = 0.07 and 0.10 as a function of frequency (100–10⁶ Hz), at a 0 V d.c. bias potential. This plot's characteristic is the manifestation of a plateau in the feeble- and elevated-frequency ranges, which demonstrates a shift in slope at a specific frequency.

Two areas are evident based on the electrical conductivity analysis. In the first region, conductivity exhibits the presence of a peak that is frequency-independent and corresponds to the dc conductance. This region is found at a feeble frequency. The curves display a linear variation in the plateau region, where our compounds display semiconductor, at a 0 V d.c. bias potential [14]. The second

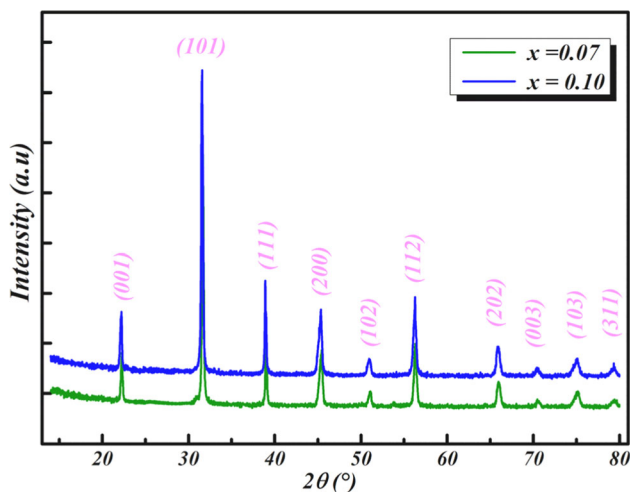


Fig. 2 XRD data for $\text{Ba}_{0.97}\text{La}_{0.02}\text{Ti}_{1-x}\text{Nb}_{4x/5}\text{O}_3$, ($x = 0.07$ and 0.10) perovskite ceramics, respectively

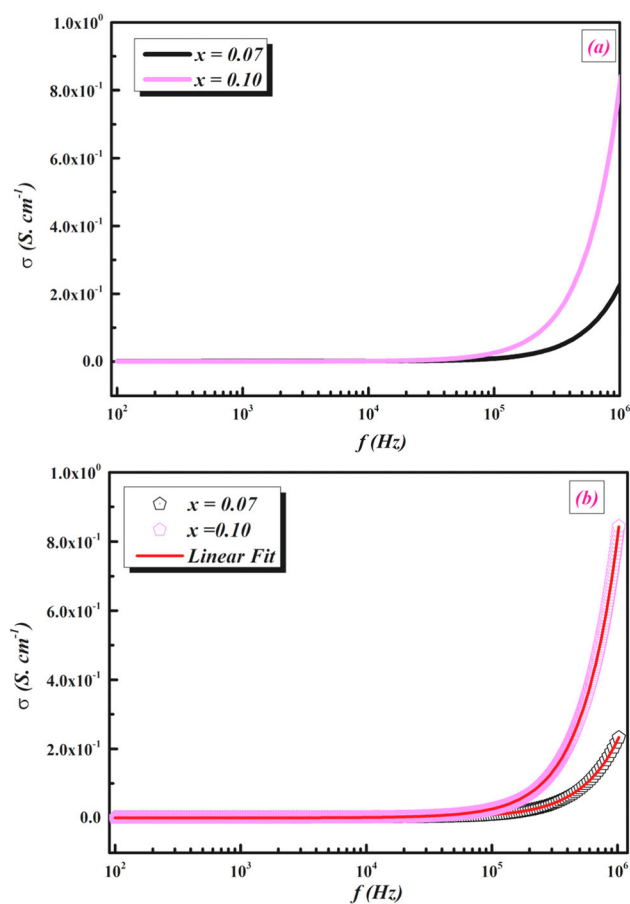


Fig. 3 (a) The variation of the total conductivity (σ) vs. frequency (b) Fitting of the experimental data, for $\text{Ba}_{0.97}\text{La}_{0.02}\text{Ti}_{1-x}\text{Nb}_{4x/5}\text{O}_3$, ($x = 0.07$ and 0.10) perovskite ceramics, at a 0 V d.c bias potential

area, which corresponds to the ac conductance, is located at a high frequency. Ac conduction plots that exhibit a shift in slope, with rising frequency.

The arcs in this field undergo a monotonous transformation and become linear. The Jonscher's universal power law is used to study the conductivity spectra [15].

$$\sigma(\omega) = \sigma_{\text{dc}} + \sigma_{\text{ac}} \quad (1)$$

In the following equation, $\sigma_{\text{tot}}(\omega)$ represents the total electrical conductivity, σ_{dc} the d.c. conductivity, and σ_{ac} the ac-conductivity:

$$\sigma(\omega) = \sigma_{\text{dc}} + A\omega^n \quad (2)$$

where A is the pre-exponential component that changes with temperature, ω is the angular frequency of the applied ac field, and 'n' is the frequency exponent that changes with frequency and temperature with a 0 to n to 1 relationship.

According to Funke [16], for $n \leq 1$, the motion involves localized hopping without species fleeing the neighborhood sides, whereas for $n > 1$, the motion involves translational motion with a sudden hopping of charge carriers. Although this measure is frequency-independent, it is also temperature- and material-dependent.

Figure 3b illustrates via Eq. (2) matched the experimental data of total conductivity vs. frequency for the $\text{BLTi}_{0.93}\text{Nb}_{0.056}$ and $\text{BLTi}_{0.90}\text{Nb}_{0.08}$ samples, at 0 V d.c-bias potential. In order to discover a suitable fit for the experimental data obtained across the entire frequency part, the (A) and (n) factors were varied simultaneously in the fitting method. It is clear that the fitting process closely matches the experimental results. Table 1 contains a summary of σ_{dc} , A and n fitting values.

This graph makes it clear that the exponent n rises as the Nb concentration does. A thermally activated process is represented by the change of n with the modification of frequency. The relationship between n and frequency sheds light on the appropriate process underlying ac-conductivity.

As shown by the SEM of $\text{BLTi}_{0.93}\text{Nb}_{0.056}$ and $\text{BLTi}_{0.90}\text{Nb}_{0.08}$ micrographs, which we have essentially demonstrated these behaviors in our obviously work [11, 17], in such a situation of nonlinear fitting, the exponent n is slightly superior to 1, indicating that the hopping which occurs between neighboring sites is probably due to strongly connected grains.

Table 1 The fitting estimations of σ_{dc} , A and n $\text{BLTi}_{0.93}\text{Nb}_{0.056}$ and $\text{BLTi}_{0.9}\text{Nb}_{0.08}$ perovskite ceramics

Compounds	σ_{dc}	A	n
$\text{BLTi}_{0.93}\text{Nb}_{0.056}$	5.02568×10^{-5}	5.64875×10^{-7}	1.03
$\text{BLTi}_{0.90}\text{Nb}_{0.08}$	4.5808×10^{-5}	4.55802×10^{-7}	1.11

3.3. Dielectric study

Figure 4a shows the variation of the dielectric constant (ϵ') of Ba_{0.97}La_{0.02}Ti_{1-x}Nb_{4x/5}O₃ (for x = 0.07 and 0.10) in the frequency range of 100–10⁶ Hz, at a 0 V d.c.-bias potential. For both ceramics, (ϵ') has an elevated value at 10² Hz, a feeble frequency. This comportment shows that these structures contain all systems of disparate kinds of polarization, including dipolar, electronic, interfacial, ionic and atomic polarization [18].

On the other hand, the heterogeneous conduction in the grain and the grain boundary can also account for this large estimate of the dielectric constant (ϵ') for our compositions at feeble-frequency part. A considerably upper resistivity can be found in the grain boundary region.

Depending on the frequency, the variation of (ϵ') can be explained using the MW-type interfacial polarization principle (space charge), according to which, when an external electric field is present, the grain-to-grain

boundaries of a dielectric contribute to the polarization of the space charge, which results in a localized accumulation of the space charge [19].

The electric dipoles have a tendency to point themselves in the direction of the applied electric field with rising frequency ($\geq 10^2$ Hz). In the areas of elevated frequencies, only dipolar and space-charge polarization contribute to polarization, which causes the dielectric constant to reduce [20].

The value of (ϵ') tends to decline as frequency rises due to the charge carriers' motion of reorientation, and all polarization processes cannot behave in accordance with the direction of the applied electric field. Similar results for other ceramics were found for this demeanor [21].

Furthermore, (ϵ') at x = 0.07 is higher than that at x = 0.10. The rise in conductivity (from 7 to 10 mol% of niobium) that results in an increase in the number of available charge carriers that can move between sites explains this character. The possible use of this elevated

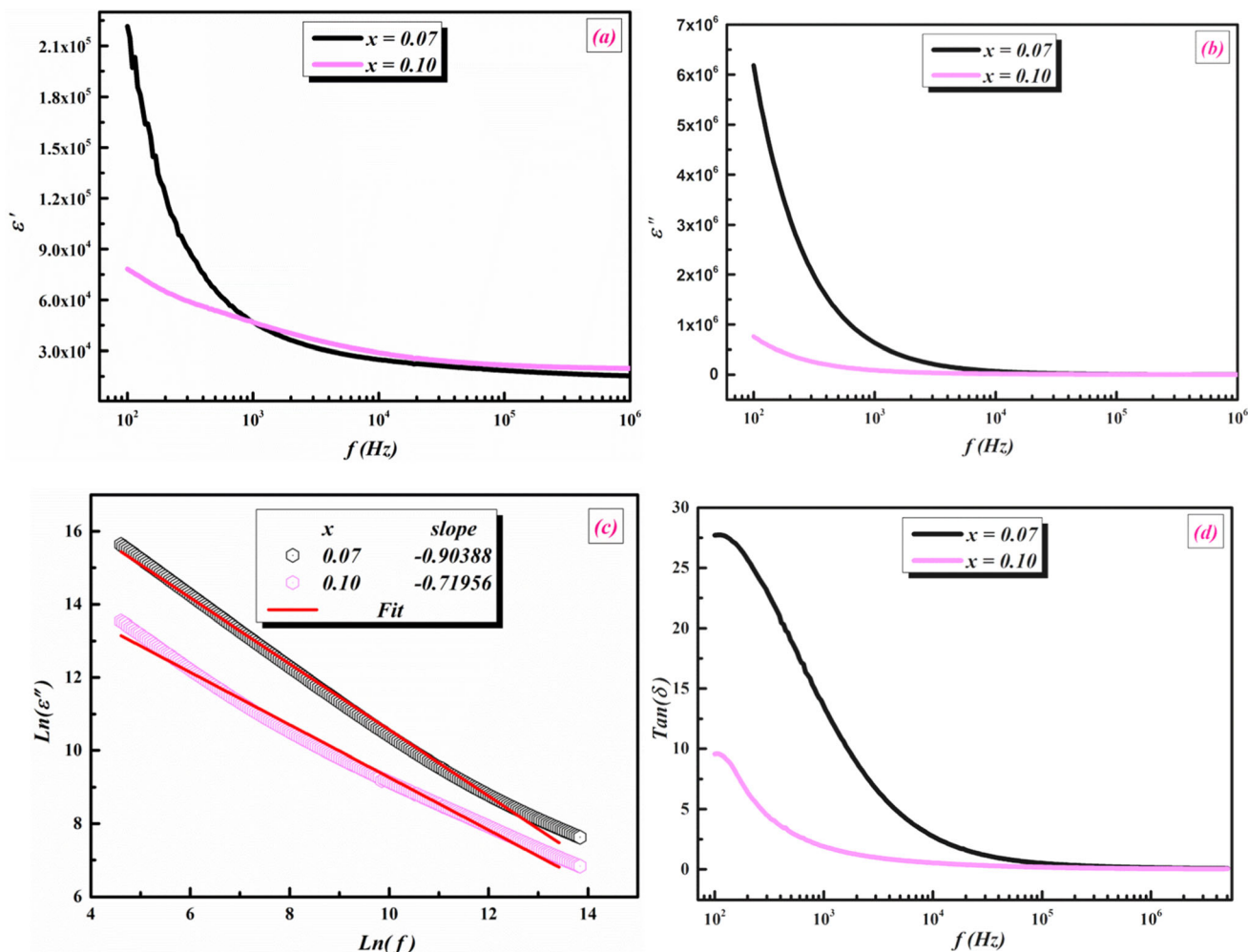


Fig. 4 The variation of (a) the real part (ϵ'), (b) the imaginary part (ϵ'') and (c) $\text{tan}(\delta)$ vs. frequency (d) The plot of $\text{Ln}(\epsilon'')$ vs $\text{Ln}(f)$ for Ba_{0.97}La_{0.02}Ti_{1-x}Nb_{4x/5}O₃, (x = 0.07 and 0.10) perovskite ceramics, at a 0 V d.c. bias potential

permittivity value in multilayer ceramic capacitors (MLCC) [22], thermistors with positive temperature coefficients [23] and other electronic components has led to a lot of interest in this property.

Figure 4b shows the variation of imaginary part of dielectric constant (ϵ'') for $\text{BaLTi}_{1-x}\text{Nb}_{4x/5}\text{O}_3$'s, for $x = 0.07$ and 0.10 , respectively, with frequency [$100\text{--}10^6$ Hz], for a potential of 0 V d.c. bias. In accordance with the dipolar polarization, (ϵ'') rises at low frequencies [24]. When frequency is high, (ϵ'') falls.

We have stated using the following equation, which is typically applied at weaker frequencies [25], that dc conductivity dominates the dielectric response of our materials, causing the relaxation phenomenon to vanish in (ϵ'') spectra.

$$\epsilon''(\omega) = \frac{\sigma_{\text{DC}}}{\epsilon_0 \omega} \quad (3)$$

Resting on Fig. 4c, it can be seen that dispersion happens at feeble-frequency values with a relatively elevated dielectric constant than at greater frequencies, where the dielectric constant reduces.

For $x = 0.07$ and 0.10 samples, we present in Fig. 4c the variation of $\ln(\epsilon'')$ against $\ln(f)$ at a 0 V d.c.-bias potential. Certain oxides have shown this type of comportment [26]. The slope of the adjusted plot between $\ln(\epsilon'')$ and $\ln(f)$, plotted for our data, was established to be -0.90388 and -0.71956 for $x = 0.07$ and 0.10 , respectively.

The curve disproves the existence of any Debye-type dipole loss point. $\text{Ba}_{0.97}\text{La}_{0.02}\text{Ti}_{1-x}\text{Nb}_{4x/5}\text{O}_3$ (for $x = 0.07$ and 0.10) ceramic compositions have straight lines with slopes that are near to 1, indicating that the dc conduction mechanism is the dominant one [27].

Figure 4d illustrates the changes in the loss tangent ($\tan \delta$) vs. frequency (f), for a potential of 0 V d.c. bias. This graph unequivocally demonstrates a relaxation apex. With the addition of Nb to our sample, the displacements on the high-frequency side allowed us to prove the Maxwell–Wagner polarization's existence [28].

The observed comportment in the feeble-frequency region suggests that relaxor dielectric demeanor is present in both of the analyzed perovskite ceramics. Space-charge polarization, which happens when two grain-grain boundaries phases of varying electrical conductivity are in contact, may be responsible for the feeble-frequency relaxation [29]. Then again, the greater density of the charge carrier might be the cause of this raising. The dielectric loss reduces and stays constant at elevated-frequency values. The drop in resistance is responsible for the reduction in dielectric loss, for a potential of 0 V d.c. bias [30].

3.4. Electric study

For $x = 0.07$ and $x = 0.10$, respectively, Fig. 5a depicts the variation of the real part of impedance (Z') against to frequency within the range of $100\text{--}10^6$ Hz, for a potential of 0 V d.c. bias. For both perovskite ceramics, (Z') has the uppermost value at weaker frequency, diminishes with rising frequency, and merges at elevated frequency. This outcome is a consequence of the material's space-charge polarization being released [31].

For a particular frequency, it is discovered that (Z') value rises as Niobium concentration rises. The reducing in space-charge accumulation at the grain boundaries is ascribed to this attitude. It exhibits the characteristic negative temperature coefficient of resistance thermistors (NTC thermistors) behavior [32] of $\text{Ba}_{0.97}\text{La}_{0.02}\text{Ti}_{1-x}\text{Nb}_{4x/5}\text{O}_3$, (for $x = 0.07$ and 0.10) ceramic samples and may therefore be linked to increased ac-conductivity nil d.c.-bias potential (Fig. 3).

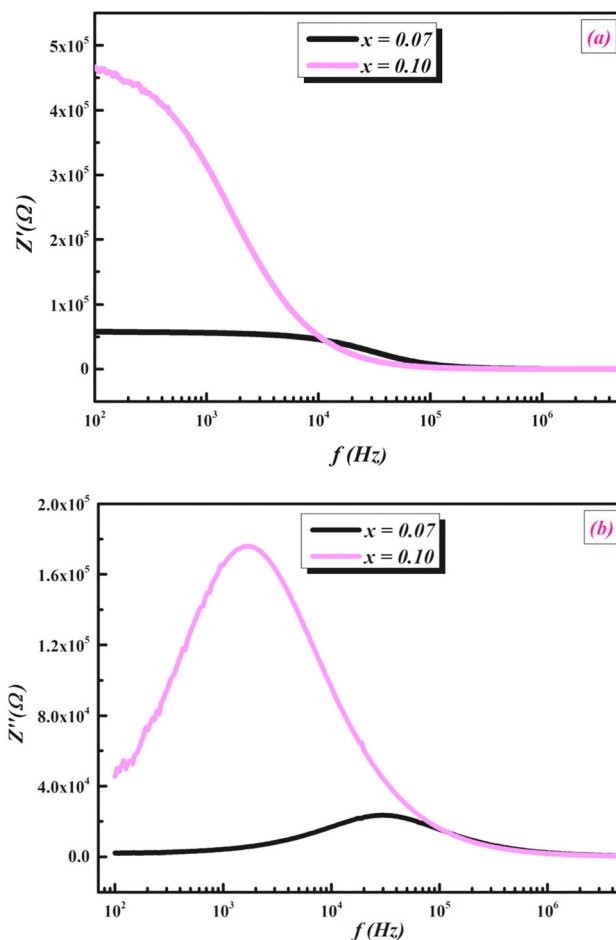


Fig. 5 The variation of (a) the real part (Z'), (b) the imaginary part (Z'') vs. frequency for $\text{Ba}_{0.97}\text{La}_{0.02}\text{Ti}_{1-x}\text{Nb}_{4x/5}\text{O}_3$, ($x = 0.07$ and 0.10) perovskite ceramics, at a 0 V d.c. bias potential

Figure 5b shows the frequency-dependent evolution of the imaginary part of impedance (Z''), at a 0 V d.c. bias potential, with different Nb amounts. The curves prove that for $x = 0.07$ and 0.10 , the (Z'') values reach their maximum apex (Z''_{\max}) at what is known as the electrical relaxation frequency (f_{\max}). With $x = 0.07$, the value of (Z''_{\max}) changes to superior frequencies, and with $x = 0.10$, it shifts to weaker frequencies.

It is possible to see a typical apex broadening that is slightly asymmetrical in character. The merger of Z'' in the important frequency area might be a sign that a space-charge relaxation is taking place. When the system is made of grains and grain boundaries, space-charge polarization predominates [33]. Furthermore, the decline in (Z'') is described by the decline in resistive part of the ceramics.

Figure 6a displays the Nyquist graphs (Z'') against (Z') for $x = 0.07$ and 0.10 , at a 0 V d.c. bias potential. The manifestation of a semi-circular arc at elevated and middle frequencies, followed by a linear segment at weaker frequency, characterizes our spectra systems. With rising niobium rates, the visible semicircle's diameters shrank noticeably.

The rise in space-charge accumulation at grain boundaries is responsible for this performance. The upper frequency spectrum is connected to the semicircle that is nearest to the origin, and it is primarily due to impedance brought on by electronic transport.

The electrochemical impedance spectroscopy (EIS) spectra analyzer [34], a potent method to ascertain the input of electrode or electrolytic processes to these systems, was used to match the experimental data of Nyquist plots. The dynamics of linked or mobile charges on the volume of interface areas or any liquid or solid materials can also be studied using it [35].

An equivalent circuit, depicted in the inset of Fig. 6b, models $x = 0.07$ and 0.10 , at a 0 V d.c. bias potential. Two R//CPEs (R-resistance and CPE-constant phase element) are connected in series in this circuit.

The distribution of relaxation times can be related to the constant phase element, which is a non-ideal frequency-dependent capacitance [36]. The CPEi numbers show a departure from a pure capacitor. CPE-T1 and CPE-T2 have values that are less than 1. These values are meant by the term "CPE impedance" as:

$$Z_{\text{CPE}} = \frac{1}{A(j\omega)^P} \quad (4)$$

where $P = 0$ and $P = 1$ represented the CPE as a resistor and ideal capacitor, respectively [37]. Table 2 displays the equivalent circuit's fitted parameters. The results clearly indicate the semiconducting nature of Ba_{0.97}La_{0.02}Ti_{1-x}Nb_{4x/5}O₃, (for $x = 0.07$ and 0.10) ceramics.

3.5. Electrical modulus study

At a 0 V d.c.-bias potential, the frequency dependence of real part of dielectric modulus (M') is shown to have a broad frequency range of in Fig. 7a, BLTi_{0.93}Nb_{0.056} and BLTi_{0.90}Nb_{0.08} perovskite samples. With frequency, (M') rose in value and displayed a dispersion that tended toward (M_{∞}) (M' 's asymptotic value at elevated frequencies). At weaker-frequency values, (M') was discovered to be extremely low (just about zero), and it showed a rising tendency as frequency rose. It displayed continuous dispersion with rising frequency.

This dispersion might be caused by a conduction attitude brought on by charge carriers' short-range movement when subjected to an induced electric field [38]. The character of the variation suggested that the bulk (Intragrains) of the materials is what gives origin to the electrical properties. This suggests that the flow of charge under the effect of a constant electric field is not subject to a restoring force.

Figure 7b illustrates the imaginary part of the electric modulus (M'') varies with frequency for $x = 0.07$ and 0.10 at a 0 V d.c. bias potential. A singular relaxation apex that appears at a specific frequency defines these curves. Moreover, it is evident that as the concentration of doping rose, the magnitude and location of the peaks moved toward the elevated-frequency side.

The variation in our compounds' microstructure and cation distribution is correlated with the variation in the apex position of the imaginary part of the modulus [39]. The range of frequencies in which charge carriers can travel from one site to the neighboring site over a great distance is represented by the (M'') apex when it shows on the weaker-frequency side.

The frequency range, in which the charge carriers cannot traverse their potential wells and their motion may be within the well, however, is indicated by the appearance of the (M'') apex on the elevated-frequency side [40].

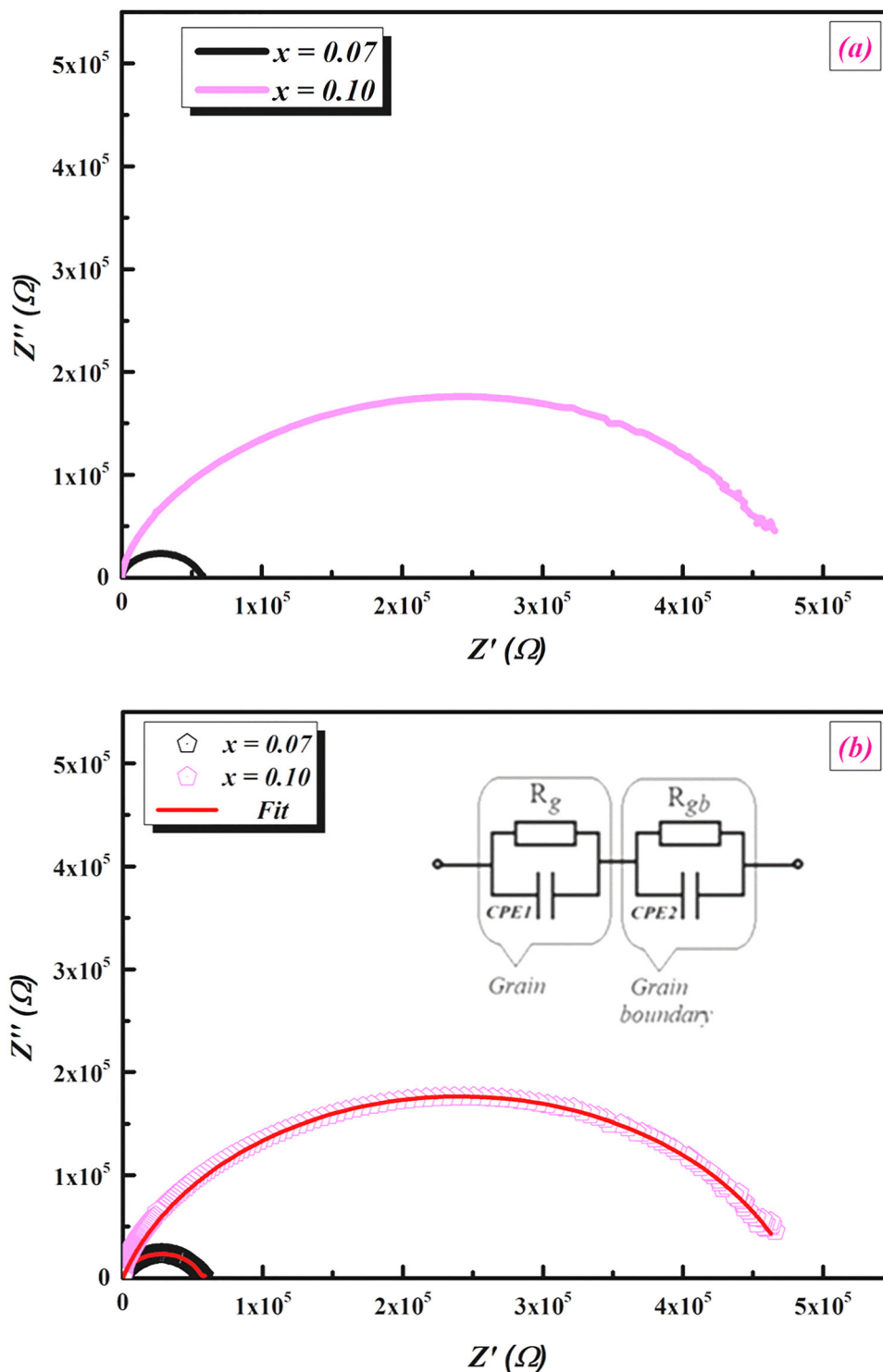
As a result, our study shows that the mobility of charge carriers transitions from long to short range with a raise in frequency. A non-Debye type of relaxation is therefore seen in the material [41], as indicated by the peak broadening with various time constants.

We can apply the Kohlrausch-Williams-Watts (KWW) function to match the (M'') curves [42]:

$$M''(f) = \frac{M''_p(f)}{1 - \beta + (\beta/(1 + \beta)) \left[\beta(f_p/f) + (f/f_p)^\beta \right]} \quad (5)$$

where M''_p is the peak maximum, f_p is the peak frequency of the imaginary component of the modulus, and K is the well-known Kohlrausch parameter. This parameter

Fig. 6 (a, b): The Cole-Cole plot Z'' vs. Z' for $\text{Ba}_{0.97}\text{La}_{0.02}\text{Ti}_{1-x}\text{Nb}_{4x/5}\text{O}_3$, ($x = 0.07$ and 0.10) perovskite ceramics, at a 0 V d.c bias potential



represents the amount of non-Debye behavior ($0 \leq \beta \leq 1$, $\beta = 1$ for Debye relaxation) [43].

Figure 7c illustrates an excellent accord between the theoretical calculation and the experimental data after applying the aforementioned equation. The numbers of β that can be obtained is not equal to one. The non-Debye character of the samples is indicated by the fitted values of,

which are found in the range of 0.51523 to 0.9897. A strong interaction between the charge carriers is indicated by a large value for the β parameter.

At a 0 V d.c. bias potential, the Cole–Cole curve (M'' against M'), for $x = 0.07$ and 0.10 , is displayed in Fig. 7d. When attempting to distinguish relaxation effects from

Table 2 The fitted parameters (R, CPE-Pi and CPE-Ti) of the equivalent circuit for BLTi_{0.93}Nb_{0.056} and BLTi_{0.9}Nb_{0.08} perovskite ceramics

Samples	BLTi _{0.93} Nb _{0.056}	BLTi _{0.9} Nb _{0.08}
R ₁ (Ω)	8173.6	4.8094 ^{E5}
R ₂ (Ω)	55,120	69,978
CPE ₁	6.0743 ^{E-10}	2.0532 ^{E-09}
CPE ₂	3.7902 ^{E-10}	1.1748 ^{E-09}
CPE-T ₁	0.50135	0.76851
CPE-T ₂	0.8886	0.80578

grains (conducting areas) and grain boundaries (resistive plates) in systems, the Cole–Cole plot of modulus performs better than the Nyquist plot of impedance.

In our compounds with the dominant effect of grains, Fig. 7d depicts a single semicircle, and the start of the second semicircle indicates the presence of both the grain and grain boundary contributions. The semicircle of grain

border is therefore insignificant in comparison with the semicircle of grains [44].

It is demanding to acquire two complete semicircles for grains and grain boundaries on the same scale in the impedance plot due to the significant difference (orders of magnitude) between the resistive values of grains and grain boundaries. When materials have essentially comparable resistance but different capacitance, which affirms that the complex modulus analysis is appropriate tool [45].

3.6. Normalization curves

Normalized impedance imaginary part (Z''/Z''_{\max}) and electric modulus (M''/M''_{\max}) were plotted vs. frequency, at a 0 V d.c-bias potential, in order to determine the impedance response, as shown in Fig. 8a, b, for x = 0.07 and 0.10, respectively.

For both the (Z''/Z''_{\max}) and (M''/M''_{\max}) graphs, only one apex was identified. An indication of local conduction and departure from an ideal Debye compartment is the

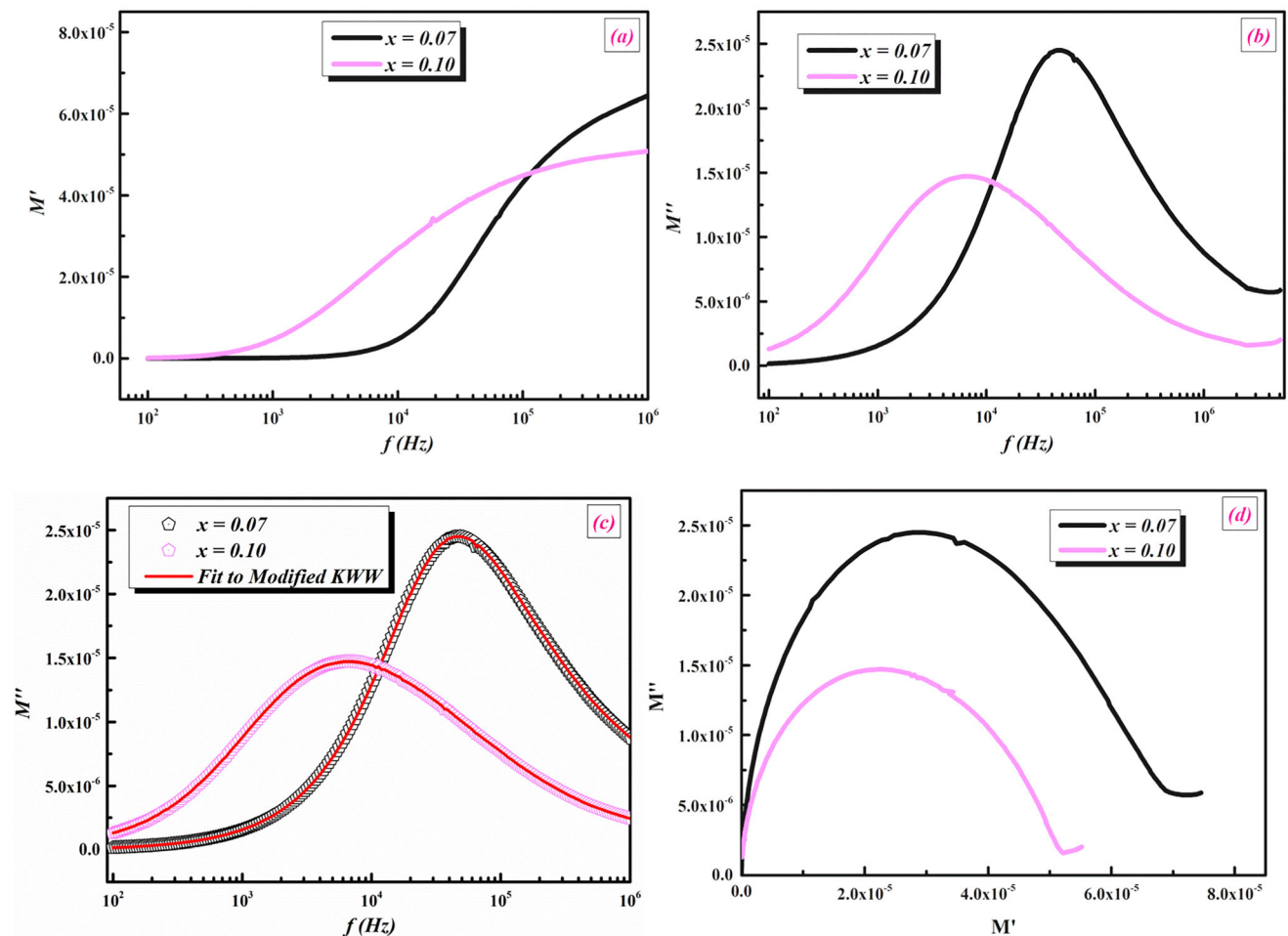
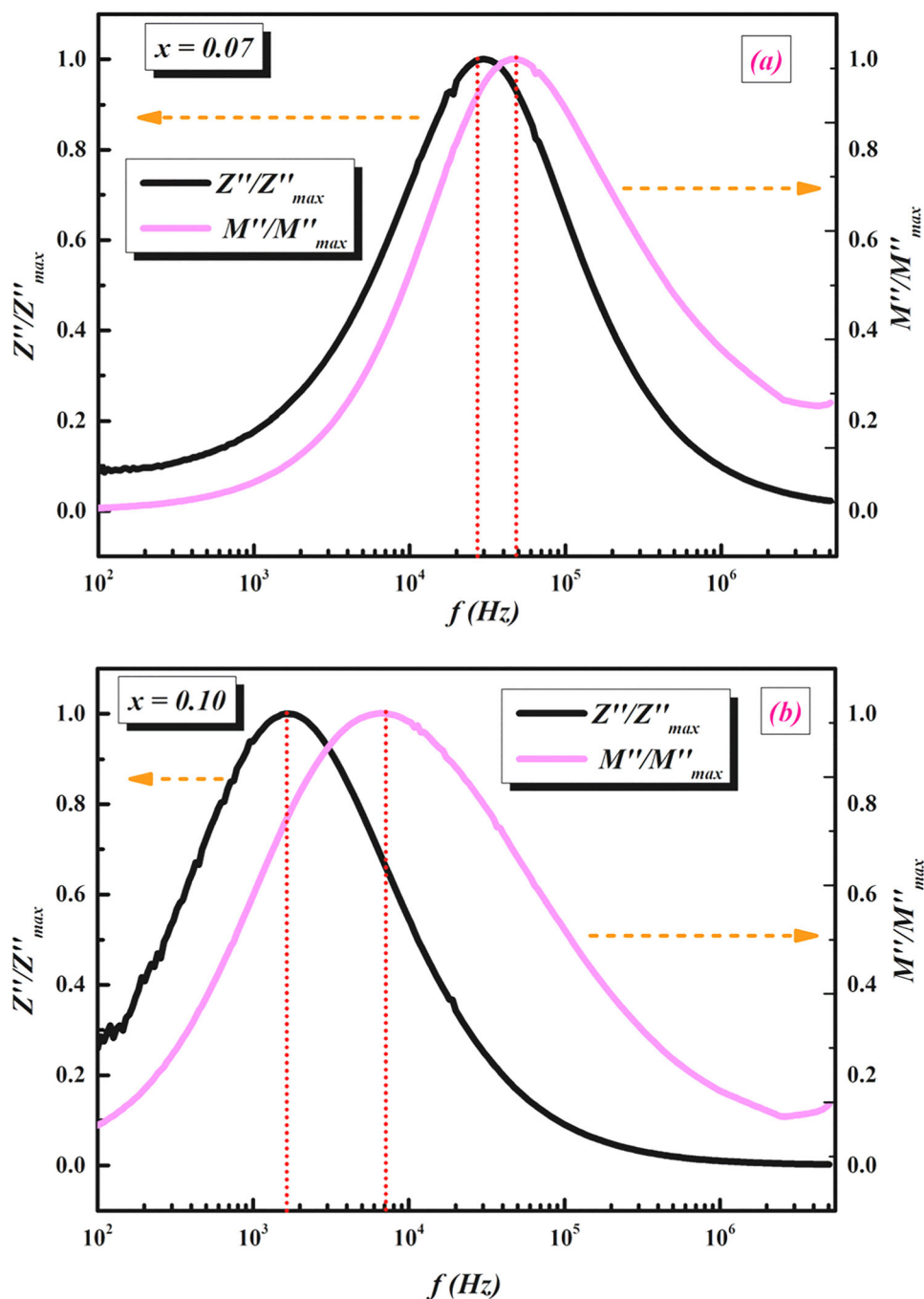


Fig. 7 The variation of the real part (M') (a), the imaginary part (M'') (b), example of fitting line using the KWW relation (c), and the Cole–Cole plot (M'' vs. M') (d), for Ba_{0.97}La_{0.02}Ti_{1-x}Nb_{4x/5}O₃, (x = 0.07 and 0.10) perovskite ceramics, at a 0 V d.c bias potential

Fig. 8 Normalized impedance (Z''/Z''_{max}) and electric modulus (M''/M''_{max}), vs. frequency, for $\text{Ba}_{0.97}\text{La}_{0.02}\text{Ti}_{1-x}\text{Nb}_{4x/5}\text{O}_3$, ($x = 0.07$ and 0.10) perovskite ceramics, at a 0 V d.c bias potential



presence of an expected separation area between normalized (Z'') and (M'') variation with frequency [10]. When compared to the apexes frequencies of, $f_{Z''}$, in the (Z''/Z''_{max}) curve, and $f_{M''}$, in the (M''/M''_{max}) curve moved to an upper frequency region ($f_{M''} > f_{Z''}$).

By examining the degree of mismatch between the apexes of both parameters, it is possible to see a shift in the apparent polarization through these representations [46]. This will enable us to determine whether charge carriers are moving over brief or long distances during the

relaxation process. If the process has a short range, (Z'') and (M'') frequency-dependence peaks will appear at various frequency parts. Peaks do, however, appear at the same frequency for charge carrier long-range movement [47].

The mismatch between the two apexes in the elaborated ceramic perovskites indicates that charge carriers are capable of short-range motion [47]. The bulk reaction can be explained in conditions of localized (dielectric relaxation) and delocalized (ionic conductivity) relaxation processes

using the comparison of the impedance and modulus data [48].

4. Conclusions

Ba_{0.97}La_{0.02}Ti_{1-x}Nb_{4x/5}O₃ (x = 0.07, and 0.10) polycrystalline ceramics have been synthesized using a low-cost flux method. According to the results of the XRD analysis performed at room temperature, our products have a P4/mmm tetragonal single phase.

The electrical conductivity was investigated, and exploratory data were fitted using the Jonscher's universal power law. The variation of ac-conductivity shows NTCR behavior indicating semi-conductor type of material. BLTi_{1-x}Nb_{4x/5} system's small niobium substitution raises the dielectric constant and lowers tangent loss, which are in perfect accord with the tetragonal structure's presence, which was clearly visible by XRD.

Rising niobium rates are observed to augment Z' evolution. The attenuation in the space-charge collected at the grain boundaries is what is responsible for this height. A semi-circular curve at both high- and low-frequency illustrates the Nyquist plot (Z'' vs. Z').

The proper equivalent circuit was installed using the electrochemical impedance spectroscopy (EIS) spectra analyzer software. This functional circuit gathers a sequential relationship between two progressively linked R//CPE elements (R-resistance, CPE-Consistent Phase Element).

Our models' electrical characteristics deviate from the ideal Debye-like behavior and are based on the complex electric modulus. The presence of a peak that shifted toward the high-frequency side with a rise in the doping rate illustrates the imaginary part of the modulus. The variety in the microstructure and the distribution of cations are linked to this evolution. Short-range flow of charge carrier was found from the relative study of the imaginary modulus M'' and impedance Z'' with frequency. Such type of materials provides various high technological applications with many useful properties making them more attractive.

Author contributions MJ contributed to conceptualization, formal analysis, investigation, visualization, writing—original draft, review and editing. JD, MAA, HB and MHD contributed to visualization and investigation. NH contributed to formal analysis and investigation.

Funding No funding was received for conducting this study.

Data availability Derived data supporting the findings of this study are available from the corresponding author upon request.

Declarations

Conflict of interest The authors declare that they do not have any known financial interests or personal relationships that could influence the presented work.

References

- [1] H Kim, A Amarnath, J Bagherzadeh, N Talati and R G Dreslinski *ACM J. Emerg. Technol. Comput. Syst.* **17** 1 (2021)
- [2] Hiroshi Kishi, Youichi Mizuno and Hirokazu Chazono *Jpn J. Appl. Phys.* **42** 1 (2003)
- [3] Wu Tong et al *Adv. Mater.* **35** 2208121 (2023)
- [4] Quan Ding et al *J. Mater. Sci.: Mater. Electron.* **34** 1411 (2023)
- [5] U Younas et al *RSC Adv.* **13** 5293 (2023)
- [6] B V S Reddy, K Srinivas, N S Kumar, K C B Naidu and S Ramesh *Chem. Phys. Lett.* **752** 137552 (2020)
- [7] S Korkmaz and I A Kariper *J. Electroceram.* **48** 8 (2022)
- [8] C Rayssi, M Jebli, S Bouzidi, J Dhahri, H Belmabrouk and A Bajahzar *Appl. Phys. A* **128** 435 (2022)
- [9] M Jebli, C Rayssi, J Dhahri, M B Henda, H Belmabrouk and A Bajahzar *RSC Adv.* **11** 23664 (2021)
- [10] M Jebli, J Dhahri, M A Albedah, F N Almutairi and H Belmabrouk *J. Mater. Sci.: Mater. Electron.* **34** 1425 (2023)
- [11] M Jebli, N Hamdaoui, J Dhahri, H Belmabrouk, A Bajahzar and M L Bouazizi *J. Mol. Struct.* **1260** 132788 (2022)
- [12] M Jebli et al *J. Alloys Compd.* **784** 204 (2019)
- [13] Marwa Jebli et al *J. Mol. Struct.* **1254** 132238 (2022)
- [14] Filip Kilibarda et al *Adv. Electron. Mater.* **7** 2100252 (2021)
- [15] Athanasios Tiliakos, Mihaela Iordache, Mircea Răceanu and Adriana Marinou *Ceram. Int.* **49** 10588 (2023)
- [16] S Das, S Swain and R N P Choudhary *J. Solid State Chem.* **325** 124121 (2023)
- [17] Ch Rayssi et al *J. Mol. Struct.* **1249** 131539 (2022)
- [18] Walter Nsengiyumva et al *Opt. Mater.* **123** 111837 (2022)
- [19] A Rastogi, F P Pandey, A S Parmar, S Singh, G Hegde and R Manohar *J. Nanostruct. Chem.* **11** 527 (2021)
- [20] Marwa Jebli et al *J. Mater. Sci.: Mater. Electron.* **31** 15296 (2020)
- [21] Yu Chen, Huajiang Zhou, Shaozhao Wang and Qiang Chen *J. Alloys Compd.* **854** 155500 (2021)
- [22] G Kerridge, D C Sinclair and J S Dean *Acta Mater.* **207** 116690 (2021)
- [23] M Zhang, T Caldwell, A L Hector, N Garcia-Araez and J Falvey *Dalton Trans.* **52** 297 (2023)
- [24] Ali Asad et al *Materials* **14** 5375 (2021)
- [25] S Bhattacharjee, R K Parida and B N Parida *Mater. Sci. Eng. B* **271** 115234 (2021)
- [26] C Rayssi, S E Kossi, J Dhahri and K Khirouni *J. Alloys Compd.* **759** 93 (2018)
- [27] Bandana Panda *Phys. B Condensed Matter.* **583** 411967 (2020)
- [28] S Demirezen and S A Yerişkin *J. Mater. Sci. Mater. Electron.* **32** 25339 (2021)
- [29] A Sen *Appl. Phys. A* **126** 336 (2020)
- [30] S B Aziz, W O Karim and H O Ghareeb *J. Mater. Res. Technol.* **9** 4692 (2020)
- [31] S A Mazen, A S Nawara and N I Abu-Elsaad *Ceram. Int.* **47** 9856 (2021)
- [32] M Jebli, N Hamdaoui, J Dhahri, M A Albedah, H Belmabrouk and M L Bouazizi *J. Mater. Sci. Mater. Electron.* **33** 18544 (2022)
- [33] M Z Khan, I H Gul, M M Baig and M A Akram *Electrochim. Acta* **441** 141816 (2023)

- [34] S Wang, J Zhang, O Gharbi, V Vivier, M Gao and M E Orazem *Nat. Rev. Methods Primers* **1** 41 (2021)
- [35] F Kubannek and U Krewer *J. Electrochem. Soc.* **167** 144510 (2020)
- [36] Byoung-Yong Chang *J. Electrochem. Sci. Technol.* **13** 479 (2022)
- [37] Yujie Wang and Guangze Gao *J. Power Sour.* **449** 227543 (2020)
- [38] A A Al-Muntaser et al *Ceram. Int.* **49** 18322 (2023)
- [39] M Z Ahsan, M A Islam, A A Bally and F A Khan *Results Phys.* **17** 103172 (2020)
- [40] M M Nofal, S B Aziz, H O Ghareeb, J M Hadi, E M A Dannoun and S I Al-Saeedi *Materials* **15** 2143 (2022)
- [41] B Tiwari, T Babu and R N P Choudhary *Mater. Chem. Phys.* **256** 123655 (2020)
- [42] S Chakrabarty, S Bandyopadhyay, M Pal and A Dutta *Mater. Chem. Phys.* **259** 124193 (2021)
- [43] M Jebli, J Dhahri, M A Albedah, F N Almutairi and H Belmabrouk *J. Mater. Sci. Mater. Electron.* **34** 18 1425 (2023)
- [44] X Chang et al *J. Mater. Sci. Mater. Electron.* **34** 260 (2023)
- [45] Sharifa Nasrin et al *Mater. Chem. Phys.* **297** 127322 (2023)
- [46] M Jebli, C Rayssi, J Dhahri and M Ben Henda *J. Mater. Sci. Mater. Electron.* **32** 26786 (2021)
- [47] Marwa Jebli et al *Inorg. Chem. Commun.* **129** 108628 (2021)
- [48] S S Hota, D Panda and R N P Choudhary *J. Mater. Sci. Mater. Electron.* **34** 10 900 (2023)

Publisher's Note Springer Nature remains neutral with regard to jurisdictional claims in published maps and institutional affiliations.

Springer Nature or its licensor (e.g. a society or other partner) holds exclusive rights to this article under a publishing agreement with the author(s) or other rightsholder(s); author self-archiving of the accepted manuscript version of this article is solely governed by the terms of such publishing agreement and applicable law.